Dix et al., http://www.jcb.org/cgi/content/full/jcb.201211052/DC1

Figure S1. **Predicted secondary structures of RNA localization elements and representative protein profile for RNA affinity purification experiments.** (A–C) Predicted secondary structures of the localization signals and mutant versions used in this study, generated using mfold version 2.3 with a folding temperature of 25°C (http://mfold.rna.albany.edu). ΔG is Gibbs free energy (kcal mol^{-1}). Note all mutants harbor subtle mutations that are predicted to maintain most secondary structural features. as, antisense; SL, stem–loop. The mutants ILS^{as}, TLS^{U6C}, and $TLS^{\Delta CA}$ (a removal of C33 and A37; also known as $TLS^{\Delta bub}$ [Dienstbier et al., 2009]) were shown previously to strongly perturb the apical enrichment of localization signals in *Drosophila* embryos (Dienstbier et al., 2009). HLE^{r12} is a mutant with a GAA-to-CUU change in SL1 at positions 41–43, which abolishes apical localization of the associated *h* transcript (Bullock et al., 2003). Numbering corresponds to the nt positions within the affected stem loops. (D) Silver-stained gel showing the profile of bands observed for a typical experiment comparing proteins bound to *ILS* and the mutant ILS^{as}. The bands corresponding to Dhc, Egl, and BicD (determined by comparison with immunoblots) are marked. Additional bands with greater intensity in the *ILS* lane were also observed (examples shown with red arrows), corresponding to possible additional components of localization complexes. The band that excludes the silver stain (asterisk) is the eluted RNA.

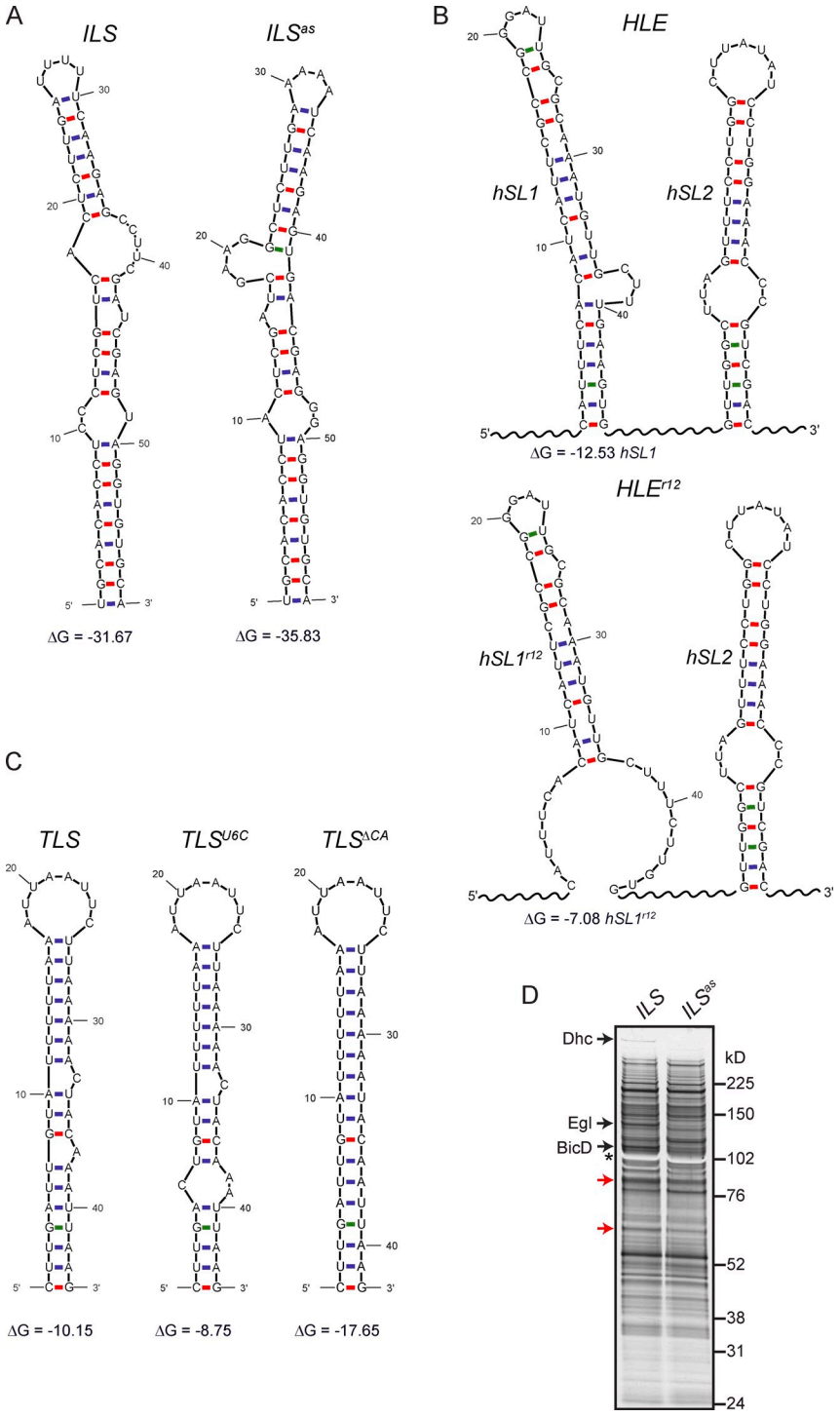

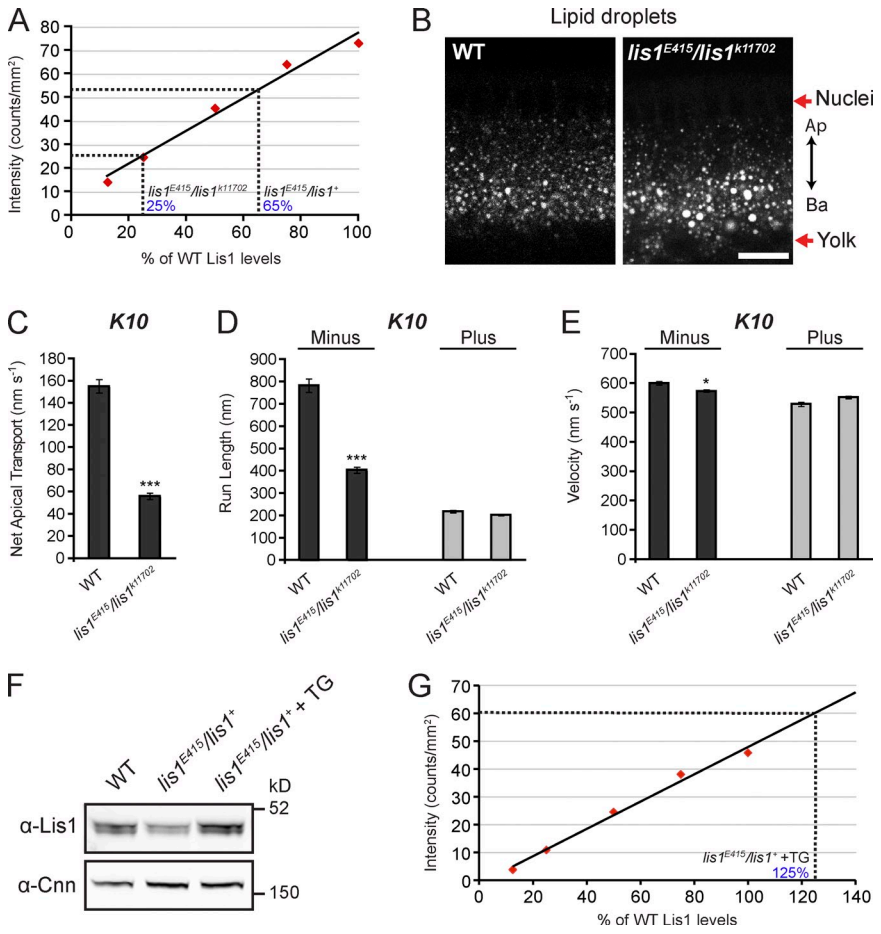

Figure S2. **Additional characterization of *lis1* mutants.** (A) Graph showing estimation of Lis1 levels in the *lis1* mutant genotypes, evaluated by fluorescent Western blotting of ovary extracts. Red diamonds show the values for Lis1 signals determined for dilutions of WT extract. The data shown are from a single experiment, although the approximate levels of Lis1 relative to WT in the mutant genotypes were verified in a second, independent experiment. (B) Nile Red staining showing the basal enrichment of lipid droplets in the peripheral cytoplasm in both WT and $lis1^{E415}/lis1^{k11702}$ embryos. Because basal enrichment of droplets is a MT-based process (dependent on kinesin-1; Shubeita et al., 2008), this result provides additional evidence that MT architecture is not perturbed in *lis1* embryos, i.e., with MT plus-ends extending basally to a similar extent as in WT. Bar, 10 µm. (C–E) Motile properties of particles of the localizing *K10* RNA after injection into the maternal genotypes as shown. For full details and number of tracks analyzed see Table S2. Statistically significant differences, which were assessed using ANOVA tests (Bullock et al., 2006), are denoted as follows: *, $P < 0.05$; ***, $P < 0.001$. (F) Fluorescent Western blotting showing that expression of two copies of a *lis1* transgene (TG) expressed under the control of the ubiquitous α-tubulin promoter increases Lis1 protein levels in $lis1^{E415}/lis1^{+}$ ovaries. Centrosomin (Cnn) is used as a control. (G) Graph showing estimation of Lis1 levels in the $lis1^{E415}/lis1^{+}$ + TG genotype, evaluated by fluorescent Western blotting of ovary extracts. Red diamonds show the values for Lis1 signals determined for dilutions of WT extract. The data shown are from a single experiment, although the approximate level of Lis1 relative to WT in the $lis1^{E415}/lis1^{+}$ + TG genotype was verified in a second, independent experiment.

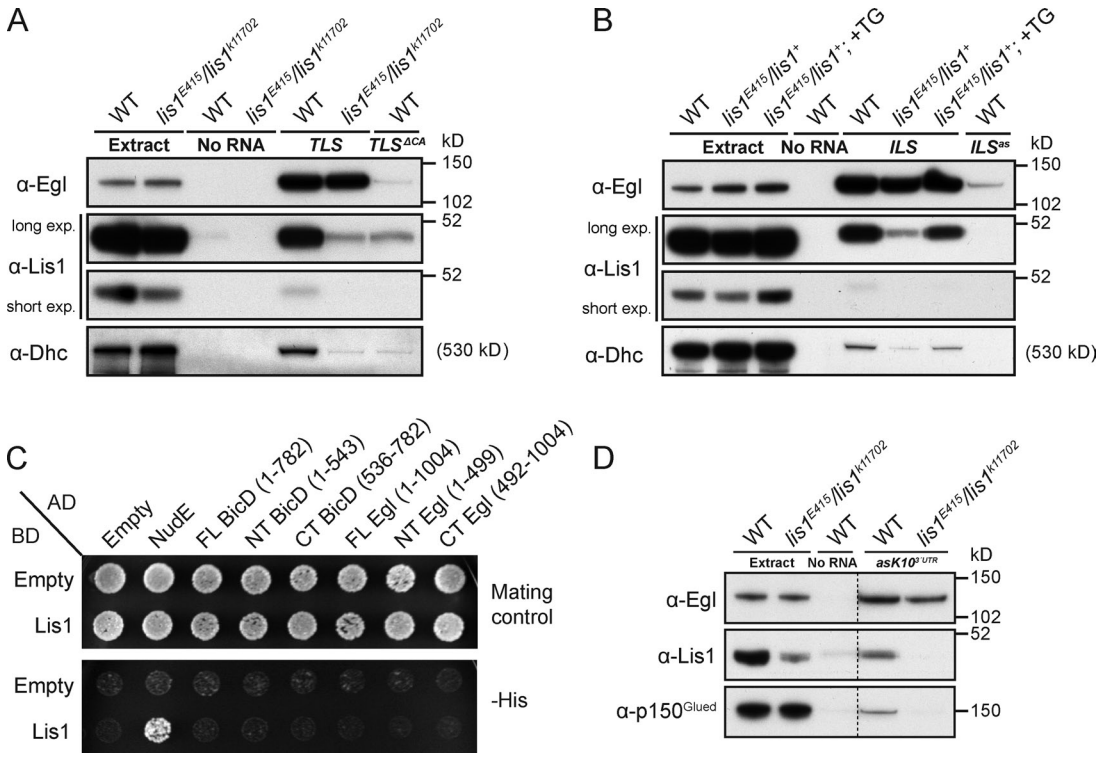

Figure S3. **Additional characterization of Lis1's role in promoting dynein–dynactin recruitment to RNAs.** (A) Immunoblots from aptamer-based RNA pull-downs showing that reduced Lis1 levels dramatically diminish the association of Dhc, but not Egl, with the *TLS*. Both long and short exposures (exp.) of the Lis1 blot are shown here, and in B, to reveal differences in Lis1 recruitment to signals, as well as Lis1 levels in the WT and mutant extracts. (B) The defective recruitment of Dhc to localization signals in the $lis1^{E415}/lis1^{+}$ mutant is suppressed by the *lis1* transgene (TG), as evidenced by aptamer-based RNA pull-downs with the *ILS* from ovary extracts. Recruitment of proteins to the ILS^{as} mutant from WT extract is shown as a specificity control. Dhc recruitment in the $lis1^{E415}/lis1^{+}$+ TG genotype does not appear to be as efficient as WT, consistent with a failure to completely suppress some parameters of RNP motility to WT levels (Fig. 4, D–F; and Table S2). We think that this may relate to an effect of overexpression of Lis1 above WT levels in this genotype (we estimate that there is 125% of WT Lis1 levels in the $lis1^{E415}/lis1^{+}$ + TG line [Fig. S2 G]). Consistent with this notion, previous work has shown that one additional copy of a wild-type *LIS1* gene in humans or 120% of WT protein levels in mice causes significant brain abnormalities (Bi et al., 2009). (C) Lis1 interacts with its known binding partner NudE by yeast two-hybrid, but not with full-length or truncated versions of Egl or BicD. Note that the Egl and BicD constructs include several used to successfully detect Egl and BicD interactions in a previous study (Dienstbier et al., 2009). AD and BD denote fusions to the GAL4 activation and DNA-binding domains, respectively ("Empty" denotes expression of these domains alone as negative controls); FL, NT, and CT denote full-length proteins, N-terminal fragments, and C-terminal fragments, respectively. (D) Immunoblots assessing protein recruitment from WT and *lis1* mutant ovary extracts to aptamer-linked $asK10^{3'UTR}$. Reduced Lis1 levels strongly decrease the association of $p150^{Glued}$, but not Egl, with this nonlocalizing RNA.

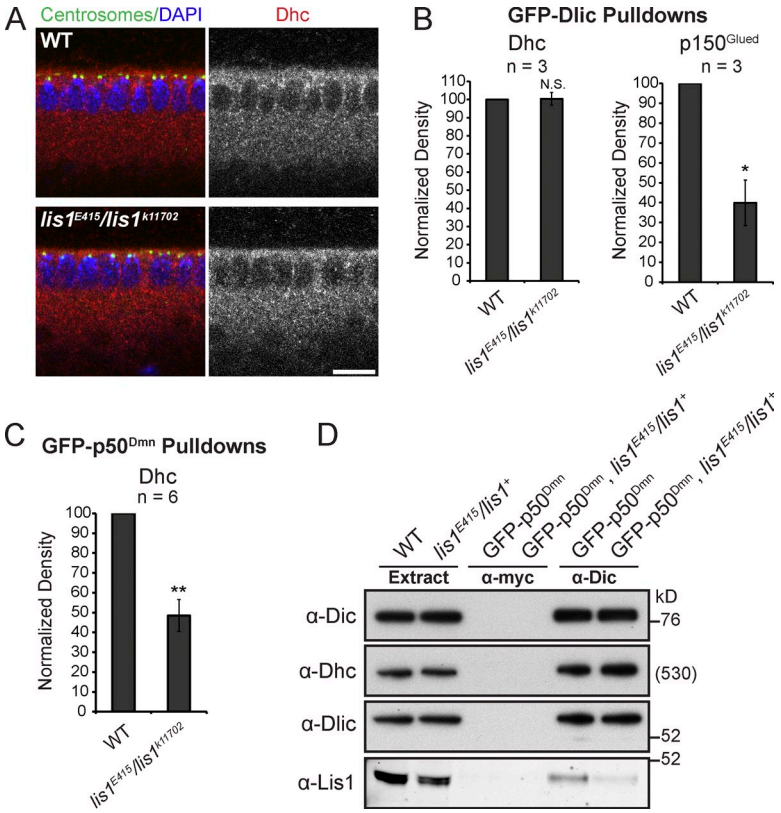

Figure S4. **Supplementary data on the role of Lis1 in promoting the association of dynein and dynactin components.** (A) Immunofluorescence images of cycle 14 embryos revealing that Dhc (red) does not form abnormal aggregates in *lis1*^{E415}/*lis1*^{k11702} mutants. Centrosomes are shown in green (α-Cnn). Nuclei are shown in blue (DAPI). Bar, 10 μm. (B) Quantification of chemiluminescent signals from immunoblots probing for Dhc or p150^{Glued} using material co-precipitated from ovary extracts with GFP-Dlic. (C) Quantification of chemiluminescent signals from immunoblots probing for Dhc using material coprecipitated from embryo extracts with GFP-p50^{Dmn}. In B and C, *n* is the number of independent pull-downs (values for Dhc and p150^{Glued} in B were determined using the same eluate run on the same membrane). Chemiluminescent signals were measured with densitometry (see Materials and methods) and values for Dhc or p150^{Glued} (B) or Dhc (C) adjusted to correct for subtle differences in the densities obtained for the GFP fusion protein in the same WT or *lis1* mutant sample. The corrected values were then expressed as a percentage of the corrected value for the same protein precipitated from the WT extract to give the normalized density value. Error bar is SEM. Statistical significance was evaluated with a one-sample *t* test (two-tailed); *, $P < 0.05$; **, $P < 0.01$; N.S., not significant. (D) Immunoblots showing that equivalent levels of Dhc and Dlic associate with dynein complexes immunoprecipitated using anti-Dic antibodies from WT and heterozygous *lis1*^{E415}/*lis1*$^{+}$ embryo extract expressing GFP-p50^{Dmn}.

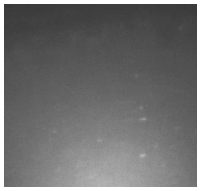

Video 1. **Composite of representative time-lapse movies of transport of Alexa Fluor 488–labeled *h* RNA in WT and *clip190*^{KO}/*Df*-null mutant embryos (tangential views).** WT, left; *clip190* mutant, right; apical (minus ends) is up and basal (plus ends) down. *h* RNA (white) accumulates apically with similar efficiency in both genotypes. RNA anchorage in the apical cytoplasm is also not inhibited in *clip190* mutant embryos. Video has a duration of 3 min 58 s and a height corresponding to 35.5 µm. One frame was captured every 297 ms with a spinning disk microscope (Ultraview ERS; PerkinElmer) equipped with a 60×/1.2 NA UPlanApo water objective. Images were captured at ∼22°C.

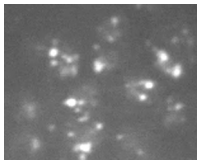

Video 2. **Composite of representative time-lapse movies of apical anchorage of Alexa Fluor 488–labeled *h* RNA in WT and *clip190*^{KO}/*Df*-null mutant embryos (apical views).** WT, left; *clip190* mutant, right. Image series of cross sections of the apical cytoplasm, beginning ∼4 min after RNA injection. In both genotypes *h* RNA puncta (white) are retained in the apical cytoplasm. Video has a duration of 37.5 s and a height corresponding to 15.5 µm. One frame was captured every 297 ms with a spinning disk microscope (Ultraview ERS; PerkinElmer) equipped with a 60×/1.2 NA UPlanApo water objective. Images were captured at ∼22°C.

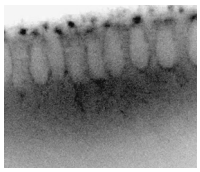

Video 3. **Composite of representative time-lapse movies of EB1-GFP, a marker of plus ends of growing MTs, in WT and *lis1*^{E415}/*lis1*^{k11702} mutant embryos (tangential views).** WT, left; *lis1* mutant, right; apical is up and basal down. Embryos had one copy of the EB1-GFP transgene. EB1-GFP is shown in black (pixel intensities were inverted to allow better visualization of the signal). In both genotypes the vast majority of dynamic plus-ends below the apical cytoplasm are growing in the basal direction. Bright EB1-GFP puncta in the apical cytoplasm are likely to correspond to a centrosomally located pool of the protein (Rogers et al., 2002). Video has a duration of 5 min and a height corresponding to 15.5 µm. One frame was captured every 748 ms (using 2 × 2 binning) with a spinning disk microscope (Ultraview ERS; PerkinElmer) equipped with a 60×/1.2 NA UPlanApo water objective. Images were captured at ∼22°C.

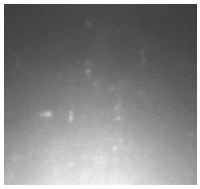

Video 4. **Composite of representative time-lapse movies of transport of Alexa Fluor 488–labeled *h* RNA in WT and *lis1*^{E415}/*lis1*^{k11702} mutant embryos (tangential views).** WT, left; *lis1* mutant, right; apical (minus ends) is up and basal (plus ends) down. In *lis1* mutant embryos *h* RNA particles (white) undergo relatively short movements in the plus- and minus-end directions, but the longer minus end–directed runs observed in WT embryos are less frequent and diminished in length. In both genotypes, RNPs that reach the apical cytoplasm are retained there. Each movie has a duration of 6 min 54 s and a height corresponding to 33 µm. One frame was captured every 297 ms with a spinning disk microscope (Ultraview ERS; PerkinElmer) equipped with a 60×/1.2 NA UPlanApo water objective. Images were captured at ∼22°C.

Table S3 is a spreadsheet showing raw and normalized spectral counts for all proteins identified by mass spectrometry in the biochemical screen, and is provided online as a Microsoft Excel file.

References

Bi, W., T. Sapir, O.A. Shchelochkov, F. Zhang, M.A. Withers, J.V. Hunter, T. Levy, V. Shinder, D.A. Peiffer, K.L. Gunderson, et al. 2009. Increased LIS1 expression affects human and mouse brain development. *Nat. Genet.* 41:168–177. http://dx.doi.org/10.1038/ng.302

Bullock, S.L., and D. Ish-Horowicz. 2001. Conserved signals and machinery for RNA transport in *Drosophila* oogenesis and embryogenesis. *Nature*. 414:611–616. http://dx.doi.org/10.1038/414611a

Bullock, S.L., D. Zicha, and D. Ish-Horowicz. 2003. The *Drosophila hairy* RNA localization signal modulates the kinetics of cytoplasmic mRNA transport. *EMBO J.* 22:2484–2494. http://dx.doi.org/10.1093/emboj/cdg230

Bullock, S.L., A. Nicol, S.P. Gross, and D. Zicha. 2006. Guidance of bidirectional motor complexes by mRNA cargoes through control of dynein number and activity. *Curr. Biol.* 16:1447–1452. http://dx.doi.org/10.1016/j.cub.2006.05.055

Dienstbier, M., F. Boehl, X. Li, and S.L. Bullock. 2009. Egalitarian is a selective RNA-binding protein linking mRNA localization signals to the dynein motor. *Genes Dev.* 23:1546–1558. http://dx.doi.org/10.1101/gad.531009

McDermott, S.M., C. Meignin, J. Rappsilber, and I. Davis. 2012. *Drosophila* Syncrip binds the *gurken* mRNA localisation signal and regulates localised transcripts during axis specification. *Biol. Open*. 1:488–497. http://dx.doi.org/10.1242/bio.2012885

Rogers, S.L., G.C. Rogers, D.J. Sharp, and R.D. Vale. 2002. *Drosophila* EB1 is important for proper assembly, dynamics, and positioning of the mitotic spindle. *J. Cell Biol.* 158:873–884. http://dx.doi.org/10.1083/jcb.200202032

Serano, T.L., and R.S. Cohen. 1995. A small predicted stem-loop structure mediates oocyte localization of *Drosophila K10* mRNA. *Development*. 121:3809–3818.

Shubeita, G.T., S.L. Tran, J. Xu, M. Vershinin, S. Cermelli, S.L. Cotton, M.A. Welte, and S.P. Gross. 2008. Consequences of motor copy number on the intracellular transport of kinesin-1-driven lipid droplets. *Cell*. 135:1098–1107. http://dx.doi.org/10.1016/j.cell.2008.10.021

Van De Bor, V., E. Hartswood, C. Jones, D. Finnegan, and I. Davis. 2005. *gurken* and the *I factor* retrotransposon RNAs share common localization signals and machinery. *Dev. Cell*. 9:51–62. http://dx.doi.org/10.1016/j.devcel.2005.04.012